

Short Communication

## Corrosion Behavior of 2Cr12MoV Turbine Steel in Early Condensate in the Presence of Acetic Acid

Jiaqiang Wei, Baiqing Zhou\*

School of Power and Mechanical Engineering, Wuhan University, No.8 South East Lake Road, Wuchang District, Wuhan City, Hubei Province, 430072, People's Republic of China

\*E-mail: [zhoubaiqing5@163.com](mailto:zhoubaiqing5@163.com)

Received: 5 December 2016 / Accepted: 29 December 2016 / Published: 12 February 2017

---

The corrosion behavior of 2Cr12MoV turbine steel in early condensate in the presence of acetic acid was studied by weight loss test, surface analysis and Potentiodynamic polarization. The results showed that acetic acid accelerate corrosion of 2Cr12MoV turbine steel to some extent. By the concentration of acetic acid in solution increased to 5 ppm, anodic polarization behavior of 2Cr12MoV turbine steel changes from active behavior to active, passive, and transpassive behavior. The critical passivation current density for 2Cr12MoV turbine steel in HAc solution is about  $78\mu\text{A}/\text{cm}^2$ , with the increase of acetic acid concentration, the active-passive transition potential moves to the negative direction and the passive zone widened. The passivation of 2Cr12MoV steel is attributed to the formation of  $\text{Fe}(\text{Ac})_2$  layer.

---

**Keywords:** Blade steel, Acid corrosion, Acetic acid, Early condensate

### 1. INTRODUCTION

Most outage hours for steam turbines are due to corrosion of low pressure (LP) blades and disks in the phase transition zone (PTZ) [1]. The original liquid phase formed in the PTZ called early condensate. The corrosion damage in LP blades and disks in the reason of early condensates with concentrated impurities formed at the PTZ. The early condensates with concentrated impurities due to the impurities concentration of non-volatile or lower volatile impurities in the liquid phase are much higher than that in vapour phase [2-3]. The organic acid in the water/steam cycle tend to concentrate in the early condensate due to their low dissociation coefficient, acetic acid (HAc) is the principal organic acid in the early condensates, the concentration of HAc ranged from 600 to 6000 ppb in the early condensate [4]. According to the investigation of impurities in PTZ [2,5], the concentration of acetic acid in the early condensate is more than 1000 times higher than that in inlet steam. Hence, the

corrosion of low pressure steam turbine in the early condensate in the presence of acetic acid deserves attention.

In the past few decades, a number of studies have been investigated the effect of acetic acid on the corrosion of metal steel in aqueous environments [6-13]. For anodic reaction, Crolet, et al., [7] suggested HAc inhibited the anodic reaction; while, Hedges, et al., [8] suggested HAc accelerate anodic reaction by solubilise  $\text{Fe}^{2+}$ . For cathodic reaction, Geogre, et al., [9] suggested cathodic reaction in a mechanism referred to as "buffering effect", HAc dissociates and provides an additional source of free hydrogen ions near the steel surface, and the only cathodic reaction remains to be reduction of hydrogen ions. However, some papers [10-13] proposed a different mechanism—"direct reduction" of HAc: the adsorbed undissociated HAc molecule is reduced at the surface (in addition to any reduction of free hydrogen ions); In addition, the layer film on the surface of metal was not demonstrated. Generally speaking, very few systematic studies have been performed in the laboratory for turbine steel corrosion in early condensate environment in the presence of acetic acid.

In the present work, the corrosion behavior of 2Cr12MoV turbine steel in solutions of various HAc concentrations was studied by weight loss test, scanning electron microscopy (SEM), energy dispersive X-ray spectroscopy (EDS), infrared spectroscopy (IR), Raman spectroscopy, and polarization curve technique.

## 2. EXPERIMENT

### 2.1 Materials And Solution

2Cr12MoV blade steel was used for this study with a chemical composition: 0.20% C, 0.21% Si, 0.76% Mn, 0.012% P, 0.011% S, 0.007% Cr, 11.89% Mo, 0.83% Ni, 0.06% Cu, and Fe balance. The coupons for weight loss test were cut into 40mm×13mm×2mm, and then a hole with a diameter of 3mm was punched for hanging. The electrodes for electrochemical tests were embedded in epoxy resin with exposed working area of 1.0 cm<sup>2</sup>. Before the weight loss test and electrochemical measurement, the coupons and working electrodes were polished on successively grades of metallographic sandpaper up to 1200 grit, then washed by deionized water and degreased with acetone.

The concentration of HAc in the solution was ranged from 0.1 to 200 ppm and the test temperature was 90°C. Besides, before the tests, the solution was deoxygenated by purging pure N<sub>2</sub> until the concentration of dissolved oxygen below 5ppb.

### 2.2 Weight Loss Test

Weight loss test was conducted in FYXD-1L autoclave. The volume of the test solution was 500mL, the stirring rate was 100rpm and the immersion time was 24h. Before the weight loss test, the coupons were first dried in a dryer until a constant weight, and then weighted using an electronic balance with a precision of 0.1 mg. After each weight loss test, the corrosion products were removed

and then dried and weighted again. The corrosion rate  $V$  of each 2Cr12MoV coupon was obtained by Equation 1.

$$V = \frac{8.76 \cdot (m_1 - m_2)}{\rho \cdot S \cdot t} \quad (1)$$

where  $V$  is the corrosion rate,  $\text{mm} \cdot \text{y}^{-1}$ ;  $m_1$ ,  $m_2$  represent the mass of coupons before and after the test, respectively, g;  $\rho$  is the steel density of 2Cr12MoV,  $7.7 \text{ g cm}^{-3}$  is used in this work;  $S$  is the exposure area of coupons,  $\text{m}^2$ ; and  $t$  is the immersion test time, h.

### 2.3 Surface Analysis

The morphologies of coupons before and after weight loss test were characterized by SEM (Zeiss Sigma). Corrosion products on the surface of corroded coupons in solution with 200 ppm HAC were analyzed by EDS, IR and Raman spectroscopy. The Energy Dispersive X-ray spectrometer was the accessory facility of FEI Quanta 200, infrared spectrometer was a NICOLET 5700 FTIR and Raman spectrometer was a RM-1000 Confocal Raman Microspectroscopy.

### 2.4 Potentiodynamic Polarization Curves

Potentiodynamic polarization curves were carried out using a CS350 electrochemical workstation, A three-electrode system was used. The 2Cr12MoV blade steel was used as working electrode, while both Pt electrodes are functioned as the counter electrode and reference electrode. It should be pointed out that in this research, Pt electrode instead of the conventional reference electrode, i.e. saturated calomel electrode or Ag/AgCl electrode, adopted as the reference electrode, the reason is that the solution conductivity in this work is too low and chloride contamination test solution due to the diffusion of chloride from the reference electrode chamber to the test cell occurred during the test. For instance, as for the test solution with 0.1ppm HAC, the conductivity at room temperature is  $2.53 \mu\text{s/cm}$ , but after the saturated calomel electrode equipped with a Luggin capillary was immersed in solution for 1h, the conductivity was significantly increased to  $18.35 \mu\text{s/cm}$ . All potentials quoted are with reference to the saturated calomel electrode at  $25^\circ\text{C}$ .

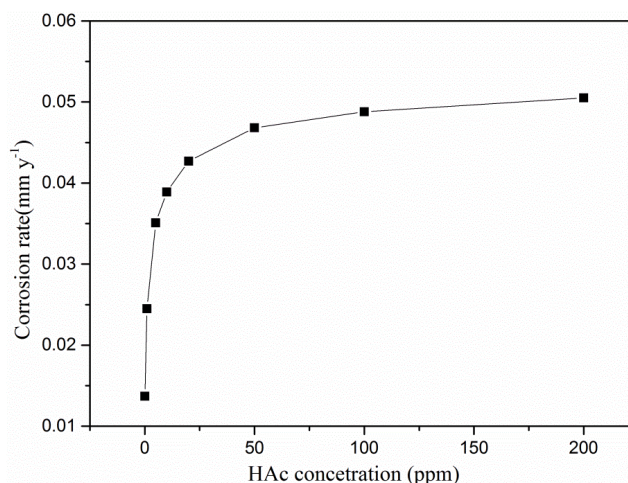
Prior to immersion of the working electrode into the test solution, the test solution was deoxygenated by purging pure  $\text{N}_2$  for 1 h. Electrode was then immersed into solution and  $\text{N}_2$  purging was continued throughout the tests at a low flow rate at the headspace but (to avoid flow effects) not bubbled through the electrolyte. Potentiodynamic polarization curves and EIS tests were conducted after reaching stable open circuit potential (OCP). The potential of polarization curves rang form -0.5 V to 2.0 V versus the OCP with a scan rate of  $5 \text{ mV} \cdot \text{s}^{-1}$ .

## 3. RESULTS

### 3.1 Weight Loss Test

Figure 1 shows the corrosion rate of 2Cr12MoV turbine steel as a function of HAC concentration. As can be seen in Fig. 1, with the increase of HAC concentration, the corrosion rate

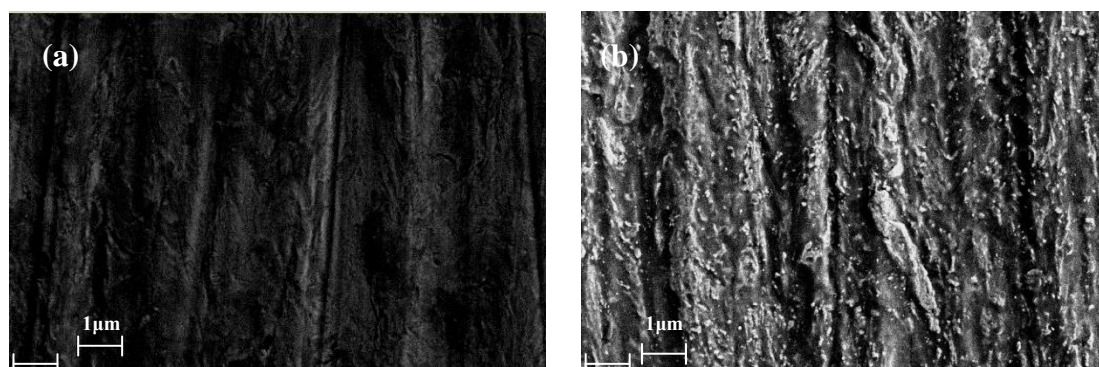
increased but the growth rate of the corrosion rate decreased. In the low HAc concentration (below 10 ppm), the corrosion rate increased rapidly from 0.014 to 0.039 mm·y<sup>-1</sup> with increasing the HAc concentration from 0.1 to 10 ppm, but increased slowly when the HAc concentration is higher than 10 ppm, and the corrosion rate is increased from 0.043 to 0.051 mm·y<sup>-1</sup> with increasing the HAc concentration from 10 to 200 ppm.



**Figure 1.** Corrosion rate of 2Cr12MoV turbine steel as a function of HAc concentration in the test solution

### 3.2 SEM Analysis

Figure 2 shows SEM micrographs of 2Cr12MoV turbine steel before and after immersion in test solution with different concentration of HAc. As shown that, corrosion products could be observed on the surface of the coupons tested. It can also be found that higher HAc concentration introduced more corrosion products on the surface, and for the coupons immersed in the test solution with 200 ppm HAc, the surface of the coupon was almost fully covered by the corrosion products, and a layer of Fe(Ac)<sub>2</sub> was formed.



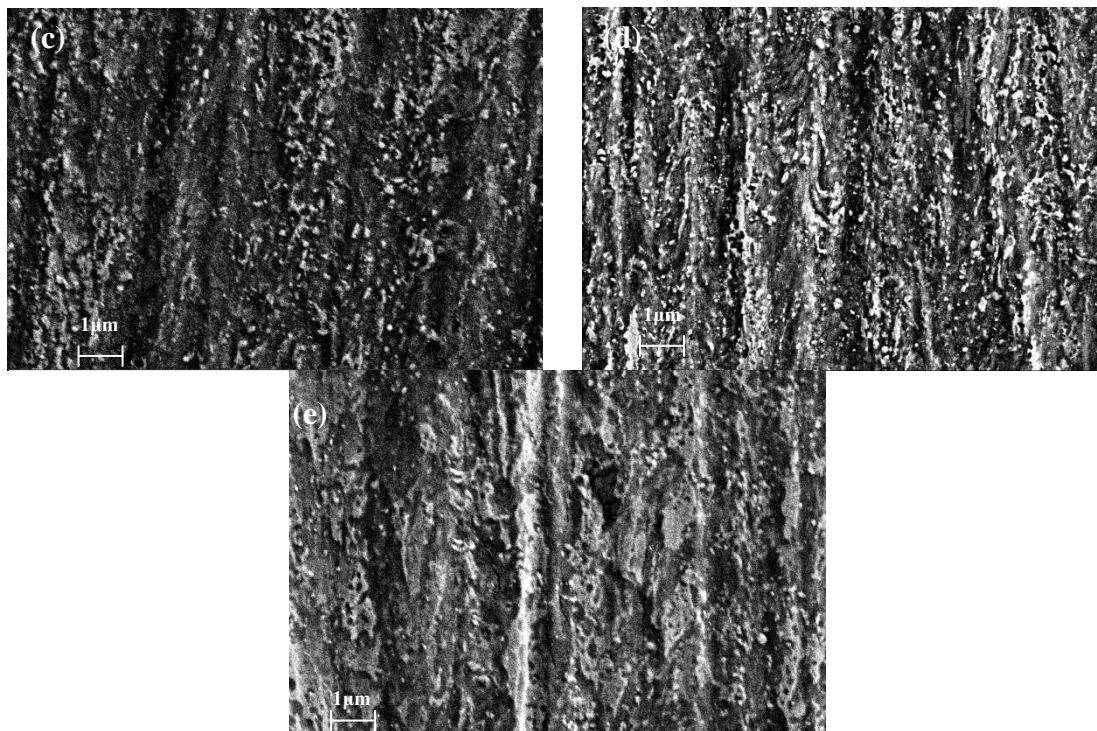


**Figure 2.** SEM surface morphologies of 2Cr12MoV turbine steel before and after immersed in the different concentration of HAc solution: (a):fresh sample before immersion, (b) 1 ppm, (c) 10 ppm, (d) 100 ppm, (e) 200 ppm.

### 3.3 EDS Analysis

Figure 3 shows the EDS spectra of corrosion products on the surface of 2Cr12MoV turbine steel immersed in test solution with 200 ppm HAc, demonstrating that the main elements of the corrosion products are consisted of Fe, O, C, Cr, and Mn. It can be indicated that the elements Cr and Mn are derived from the base metal substrate.

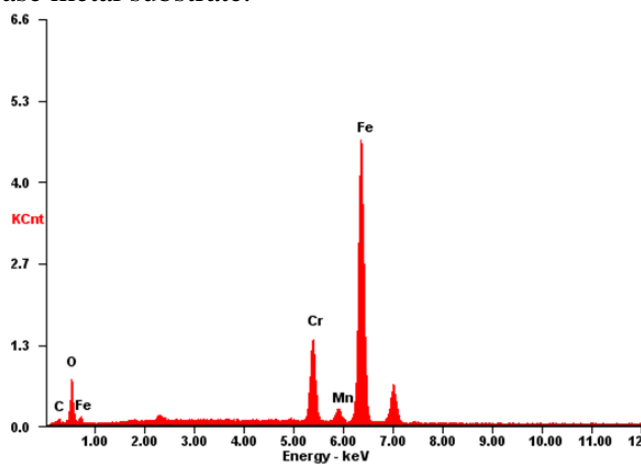


**Figure 3.** EDX spectra of corrosion products on the surface of 2Cr12MoV turbine steel immersed in test solution with 200 ppm HAc.

The atom fractions of Fe, O and C are determined to be 39.54%, 29.83% and 22.25%, respectively, in which the high atom fraction of Fe may be partially influenced by base metal substrate. The mainly elements are Fe, O, C and the atomic ratio of C and O is nearly 1:1 in consistent with the result of IR and Raman analysis which determined corrosion product was  $\text{Fe}(\text{Ac})_2$ .

### 3.4 Infrared Spectroscopic Analysis

Figure 4 shows the IR spectra of the corrosion products on the surface of 2Cr12MoV turbine steel immersed in test solution with 200 ppm HAc. There are eight characteristic bands at 1686, 1635, 1542, 1452, 1417, 1050, 910, and 668 $\text{cm}^{-1}$ , 1686 1635 and 1542  $\text{cm}^{-1}$  could be assigned to the asymmetric stretching vibration of OCO, 1452 and 1417  $\text{cm}^{-1}$  could be assigned to the symmetrical stretching vibration of OCO, 1050, 910, and 668 $\text{cm}^{-1}$  could be assigned to the out-of-plane rocking vibration of  $\text{CH}_3$ , symmetrical stretching vibration of C-C and out-of-plane rocking vibration of OCO, respectively. Thus it deduced that the corrosion products on the surface was mainly composed of  $\text{Fe}(\text{Ac})_2$  [14].

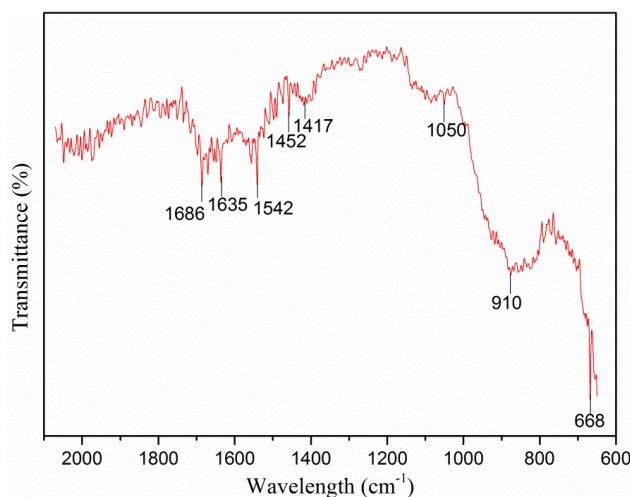


**Figure 4.** IR spectra of surface corrosion products of 2Cr12MoV turbine steel immersed in test solution with 200 ppm HAc.

### 3.5 Raman Spectroscopic Analysis

Figure 5 shows the Raman spectra of the corrosion products on the surface of 2Cr12MoV turbine steel immersed in test solution with 200 ppm HAc. It can be seen that the bands at 2945, 1597, 1409, 940 and 690 $\text{cm}^{-1}$  assigned to stretching vibration of CH of the  $\text{CH}_3$  group, stretching vibration of C=O, stretching vibration of C-O, stretching vibration of C-C, deformation vibration of OCO for  $\text{Fe}(\text{Ac})_2$ , respectively [15]. Thus the corrosion products on the surface was determined to be  $\text{Fe}(\text{Ac})_2$ .

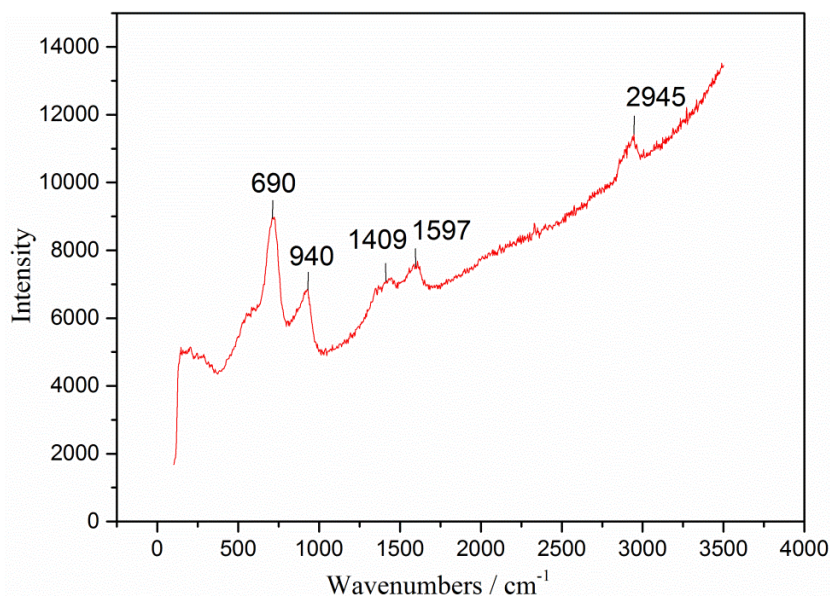


**Figure 5.** Raman spectra of surface corrosion products of 2Cr12MoV turbine steel immersed in test solution with 200 ppm HAc.

### 3.6 Polarization Curves

Figure 6 shows the polarization curves of 2Cr12MoV turbine steel in the test solution with different concentrations of HAc. The values of corrosion current ( $I_{corr}$ ), anodic Tafel slopes ( $\beta_a$ ), cathodic Tafel slopes ( $\beta_c$ ), corrosion potential ( $E_{corr}$ ), primary passivation potential ( $E_{pp}$ ), critical current density ( $i_c$ ), passivation current density ( $i_p$ ), passivation potential ( $E_p$ ), traspassivation potential ( $E_{tp}$ ) obtained from the polarization curves tested in the solutions with various HAc concentrations are summarized in Table 1.

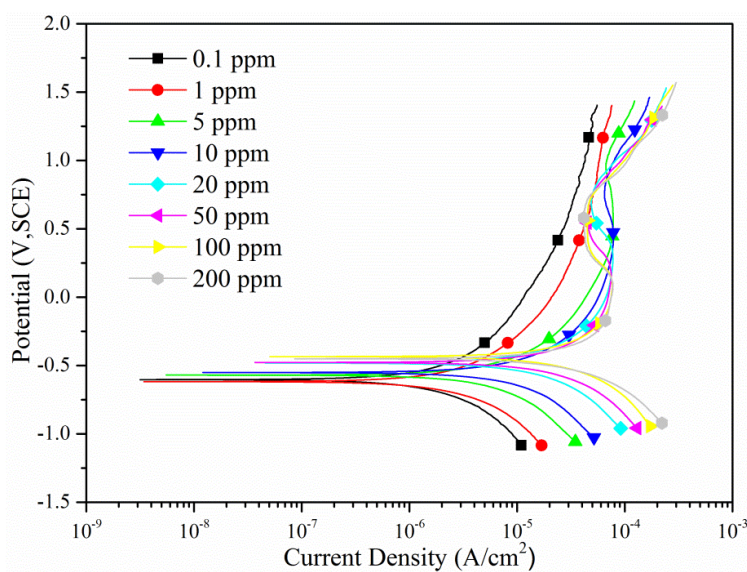


**Figure 6.** Polarization curves of 2Cr12MoV turbine steel in the different concentrations of HAc solution.

**Table 1.** Electrochemical parameters and corrosion rates of 2Cr12MoV blade steel in test solutions with different concentration of HAc based on polarization curves

Concentration of acetic acid/(ppm)	0.1	1	5	10	20	50	100	200
$I_{corr}/(\mu A \cdot cm^{-2})$	1.09	1.80	4.28	7.12	10.3	15.7	21.0	25.6
$\beta_a/(mv \cdot decade^{-1})$	378	395	404	416	437	449	456	494
$\beta_c/(mv \cdot decade^{-1})$	-315	-356	-387	-402	-407	-412	-415	-422
$E_{corr}/(mv)$	-601	-619	-577	-555	-484	-478	-450	-450
$E_{pp}/(mv)$	–	–	650	485	315	225	100	95
$i_c/(\mu A \cdot cm^{-2})$	–	–	77.5	77.9	77.5	77.9	77.5	77.5
$i_p/(\mu A \cdot cm^{-2})$	–	–	66.6	64.6	48.8	45.2	44.8	41.7
$E_p/(mv)$	–	–	925	725	645	540	445	420
$E_{tp}/(mv)$	–	–	975	805	735	700	645	630
$V/(mm \cdot y^{-1})$	0.013	0.021	0.051	0.085	0.122	0.187	0.250	0.304

As we can see from Figure 6, anodic polarization showed active behavior in the solution with the concentration of HAc lower than 1 ppm, with the concentration of HAc increased higher than 5 ppm in solution, anodic polarization converted to active, passive, and transpassive behavior. The anodic polarization curves shifted toward higher current density side at active zone and lower current density side at passive zone with increasing HAc concentration. Cathodic polarization is a hydrogen evolution and reaction mechanism independent on HAc concentration and cathodic polarization curves shifted toward higher current density side with increasing HAc concentration.

## 4. DISCUSSION

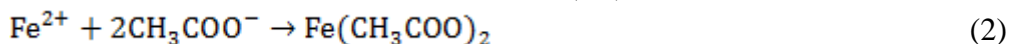
### 4.1 Weight loss test

The possible reason for corrosion rate increased with HAc concentration is that HAc increase corrosion rate by increase the concentration of  $H^+$  and solubilis  $Fe^{2+}$  [8]. At the same time, as shown in Figure 2, with the concentration of HAc increase, more corrosion products iron(II) acetate ( $Fe(Ac)_2$ ) will adsorbed on the surface of 2Cr12MoV turbine steel, which could inhibit the further corrosion and suppresses the trend of rapid corrosion. Thus, the growth rate of corrosion rate reduced with increasing HAc concentration due to more corrosion products  $Fe(Ac)_2$  adsorbed on the surface of 2Cr12MoV turbine steel with increasing HAc concentration.

### 4.2 Surface Analysis

It can be seen from Figure 2, with an increase of HAc concentration, more corrosion products adsorbed on the surface of 2Cr12MoV turbine steel. The corrosion products was determined  $Fe(Ac)_2$  by EDS, Infrared Spectroscopic and Raman Spectroscopic Analysis.

In this work, a formation mechanism for Fe(Ac)<sub>2</sub> was submitted and shown as below:



Although the solubility of Fe(Ac)<sub>2</sub> is high, but here Fe(Ac)<sub>2</sub> can adopt a polymeric structure with octahedral Fe(II) centers bridged by acetate ligands [14]. Therefore, Fe<sup>2+</sup> and CH<sub>3</sub>COO<sup>-</sup> (Ac<sup>-</sup>) seldom coexist in the form of ionic and would combine into via the formation mechanism described in Equation (2) [16]. At first, the concentration of Fe(Ac)<sub>2</sub> was low, it formed on the surface of steel and transport into solution due to its solubility high, but when the concentration of Fe(Ac)<sub>2</sub> exceeded a certain concentration in the solution and Fe(Ac)<sub>2</sub> was too late to transport away from steel surface and will adsorb on it, then in the following form a porous film of corrosion products [17]. Therefore, the higher concentration of HAC, the more corrosion products absorbed on the surface of 2Cr12MoV turbine steel.

### 4.3 Polarization Curves

The main reactions of 2Cr12MoV turbine steel in the test solution are shown as follows:



In addition, Reaction 2 occurred. With the increase of HAC concentration, the Reactions 2 tend to right direction, which indicates a higher reaction rate for Reaction 2, and Reaction 2 decrease the solubility of Fe<sup>2+</sup> promote Reaction 6. Therefore, the anodic polarization curves shifted toward higher current density side at active zone with increasing HAC concentration. Meanwhile, with the potential moved to more positive direction, more Fe<sup>2+</sup> produced by Reaction 6 are enriched near the anode surface, which promote Reaction 2, leading to more corrosion products Fe(Ac)<sub>2</sub> formed and was late to transport into solution, then absorbed on the surface of electrode. A layer formed by Fe(Ac)<sub>2</sub> when the critical current density reached during the potential moved to more positive direction and 2Cr12MoV turbine steel surface passivated. As we can see from Figure 6, there is a critical current density about 78 μA/cm<sup>2</sup> for transition from activation to passivation regardless of HAC concentration. Therefore, the increase of HAC concentration resulted in increased the Reactions (2), which induced faster Fe(Ac)<sub>2</sub> layer formed, as a result during anodic polarization the critical passivation current density was reached faster and the active-passive transition potential showed a negative shift. While, the current density of 2Cr12MoV turbine steel in the solution with HAC concentration lower than 1 ppm could not reach the critical current density during anodic polarization, thus 2Cr12MoV turbine steel could not passivate and anodic polarization showed active behavior only. Besides, the values of *i<sub>p</sub>* and *E<sub>pp</sub>* reduced, the passive zone widened with increasing HAC concentration, as shown in Table 1. M.M. Singh, et al., [17-18] also claims the passivity was attributed to the formation of salt film of Fe(Ac)<sub>2</sub> or basic iron acetate.

The cathodic reaction is a hydrogen evolution and reaction mechanism is independent on HAC concentration. With an increase in the concentration of HAC, the reaction rate of Reactions (3), (4) increased. As shown in Figure 7 and 8, corrosion rate steadily increase with a linear relationship of H<sup>+</sup>

concentration rather than HAc concentration. Therefore, cathodic reaction in a mechanism referred to as "buffering effect". HAc dissociates and provides an additional source of free hydrogen ions near the steel surface, and the only cathodic reaction remains to be reduction of hydrogen ions. This result consist with other authors' claims that HAc is not involved in charge transfer processes directly and in a mechanism referred to as "buffering effect" [19-22].

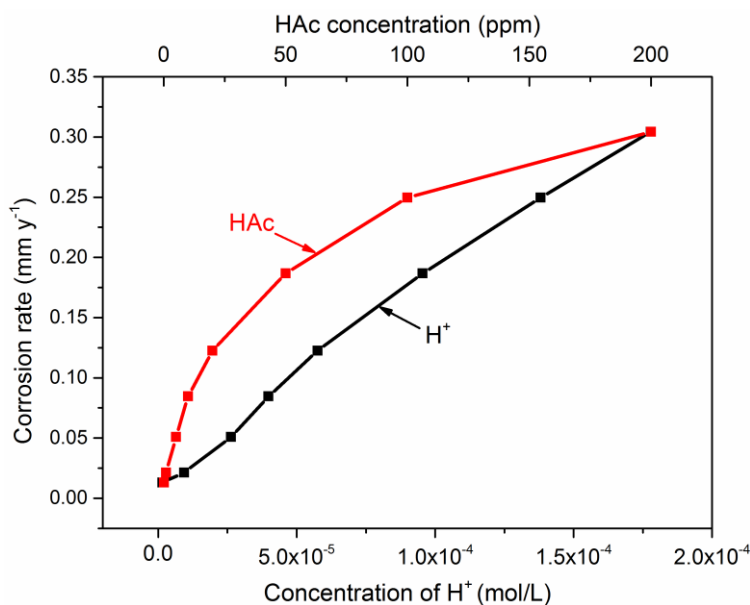


**Figure 7.** The relationship of corrosion rate obtained from polarization curves of 2Cr12MoV turbine steel with concentration of H<sup>+</sup> and HAc in test solution.

## 5. CONCLUSIONS

HAc accelerate corrosion of 2Cr12MoV turbine steel to some extent. With the increase of HAc concentration, the corrosion rate of 2Cr12MoV turbine steel increased but the growth rate of the corrosion rate decreased.

By the concentration of acetic acid in solution increased to 5 ppm, polarization behavior of 2Cr12MoV turbine steel changes form active behavior to active, passive, and transpassive behavior. The critical passivation current density for 2Cr12MoV turbine steel in HAc solution is about 78 $\mu$ A/cm<sup>2</sup> and critical HAc concentration for passivation is about 5 ppm. With the increase of acetic acid concentration form 5 ppm to 200 ppm, the values of  $i_p$  and  $E_{pp}$  reduced and the passive zone widened. The formation of Fe(Ac)<sub>2</sub> layer leads to passivation of steel in the solution. The cathodic reaction is a hydrogen evolution and in a mechanism referred to as "buffering effect".

## References

1. C. Wells, D. Rosario and B. Dooley, *EPRI.*, Report TR-111340 (1998).
2. S. Zhou, A. Turnbull, *Corros. Eng. Sci. Techn.*, 38 (2003) 7-115.
3. O.A. Povarov, T.I. Petrova and V.N. Semenov, *EPRI.*, Report TR-113090 (1999).

4. M. De Wispelaere, in: 14th International Conference on the Properties of Water and Steam, Kyoto, Japan, (2004) 602.
5. O. Jonas, Steam, *EPRI*, Report TR-108184-V1 (1999).
6. W. Y. Maeng, Digby D. Macdonald, *Corros. Sci.*, 50 (2008) 2239-2250.
7. J.-L. Crolet, N. Thevenot and A. Dugstad, *Corrosion.*, (1999) 24.
8. B. Hedges, L. McVeigh, *Corrosion.*, (1999) 21.
9. K. George, MS thesis, Department of Chemical Engineering, Ohio University, Athens, OH, (2003).
10. C. DeWaard, D. Milliams, *Corrosion.*, 31 (5) (1975) 177-181.
11. S. Nešić', J. Postlethwaite and S. Olsen, *Corrosion.*, 52 (4) (1996) 280-294.
12. L.G. Gray, B.G. Anderson and M.J. Danysh, P.R. Tremaine, *Corrosion.*, 464 (1989).
13. G. Schmitt, B. Rothmann, *Werkst. Korros.*, 28 (1977) 816-822.
14. H. G. M. Edwards, I. R. Lewis, *J. Mol. Struct.*, 296 (1993) 15-20.
15. J.K. Kim, H.S. Oh, C.W. Jo, Y.J. Suh, H.D. Jang, H.D. Jang and K.K. Koo, *Chem. Eng. Res. Des.*, 88 (2010) 1467-1473.
16. B. Weber, R. Betz, W. Bauer and S. Schlamet, *Anorg. Allg. Chem.*, 637 (2011) 102-107.
17. M. M. Singh, A. Gupta, *Corrosion.*, 56 (2000) 371-379..
18. S. K. Singh, A. K. Mukherjee, and M. M. Singh, *Indian. J. Chem. Techno.* 18 (4) (2011): 291-300.
19. T. Tran, B. Brown, S. Nesic and B. Tribollet, *Corrosion.*, 70 (3) (2014) 44-47.
20. A. Kahyarian, S. Nesic, *Electrochem. Soc. Meet. Abst.*, 12 (2015) 1067-1067.
21. A. Kahyarian, B. Brown, and S. Nešić, *Corrosion.*, 72(12) (2016) 1539-1546.
22. T.N. Tran, Doctoral dissertation, Ohio University (2014).

© 2017 The Authors. Published by ESG ([www.electrochemsci.org](http://www.electrochemsci.org)). This article is an open access article distributed under the terms and conditions of the Creative Commons Attribution license (<http://creativecommons.org/licenses/by/4.0/>).